

Behavioural analysis of iron ore tailings through critical state soil mechanics

João Paulo de Sousa Silva^{1#} , Pedro Pazzoto Cacciari² , Vidal Felix Navarro Torres³ ,
Luís Fernando Martins Ribeiro¹ , André Pacheco de Assis¹ 

Article

Keywords

Critical state
Iron ore
Laboratory tests
Numerical model calibration
NorSand
Tailings

Abstract

Understanding the geotechnical properties of iron ore tailings is currently one of the major challenges in the mining industry. With transitions from drained to undrained conditions occurring in seconds, recent dam problems have been a challenge to solve with classical soil mechanics, which provides few means to explain how such phenomena develop. There is also an increasing propensity in technical and scientific circles to seek constitutive models that are based on critical state soil mechanics and that allow for the analysis of tailings behaviour. However, there is still a lack of knowledge and information about the critical state properties of iron ore tailings. The present research experimentally and numerically investigated the effectiveness of modelling the behaviour of iron ore tailings. The aim of these experiments was to assess the critical state parameters of tailings from a significant iron ore operation site in *Quadrilátero Ferrífero* (Minas Gerais state, Brazil). The results indicated that the selected numerical model (NorSand) was adequate to evaluate the behaviour of the studied mine tailings. The numerical results showed consistent adherence to the experimental results of both drained and undrained tests, with deformations below 5% and samples in which the state parameter had a small magnitude.

1. Introduction

The first industrial iron ore extraction in Brazil occurred in *Quadrilátero Ferrífero* (QF). Today, the region remains among the most significant iron ore producers globally. The area known as QF is located in the central region of the state of Minas Gerais in Brazil. It comprises a series of hills covering approximately 7,000 km². The QF deposit was formed in the lower Proterozoic between 1.9 and 2.7 billion years ago (Dorr, 1969). With approximately 200 million tons of iron ore production per year, the QF is responsible for approximately 40% of all Brazilian iron ore production.

After many years of mineral industry operations in the QF, the region most conducive to tailings disposal has become unavailable. Many constraints hamper the utilization of conventional tailings storage facilities (TSFs) in the remaining areas. There is a need to reconcile tailings disposal and mining activities to produce lower environmental and social impacts, highlighting the importance of understanding the geotechnical behaviour of tailings (Davies, 2002). Some of these tailings have demonstrated brittle behaviour (Soga

& Mitchell, 2005; Schnaid et al., 2013), which increases the criticality of structures that are close to areas occupied by humans.

Thus, national legislation has been revised, indicating an urgent need to safely dismantle dozens of upstream tailings dams in the QF region. TSFs are among the most challenging structures to operate in the mining industry. Some of these structures are likely to be subject to piping, collapse, and flow failure and should be monitored carefully (Li et al., 2018; Olivier et al., 2018). The density and fineness of the tailings particles, which are typically uniform with little or no plasticity, usually define the behaviour of the tailings at a TSF.

Relevant research indicates that critical state theory is an attractive tool for describing the mechanical behaviour of non-cohesive soils (Dafalias & Popov, 1975; Casagrande, 1976; Jefferies, 1993; Dafalias & Manzari, 1997; Dafalias, 1986; Dafalias & Manzari, 2004; Boulanger & Ziotopoulou, 2015). The importance of this tool is highlighted by the fact that in situ soils may present a wide spectrum of states. However, obtaining undisturbed samples from noncohesive soils is complex, costly, and potentially unreliable.

[#]Corresponding author. E-mail address: eng.jpssilva@gmail.com

¹Universidade de Brasília, Brasília, DF, Brasil.

²Laboratório Geotécnico Vale, Santa Luzia, MG, Brasil.

³Instituto Tecnológico VALE., Santa Luzia, MG, Brasil.

Submitted on May 24, 2021; Final Acceptance on December 3, 2021; Discussion open until August 31, 2022.

<https://doi.org/10.28927/SR.2022.071921>



This is an Open Access article distributed under the terms of the Creative Commons Attribution License, which permits unrestricted use, distribution, and reproduction in any medium, provided the original work is properly cited.

Jefferies et al. (2015) argue that the major restriction of using the most comprehensive numerical analyses in engineering practice is the time and effort undertaken to create models. In their view, this limitation restricts the practice of engineering to commercial geotechnical modelling platforms, such as FLAC, PLAXIS, or SIGMA/W.

In the present study, the NorSand (Jefferies, 1993) model was selected because it is relatively simple and based on a small number of parameters. This model is a generalized critical state model based on the state parameter (ψ).

$$\psi = e - e_c \quad (1)$$

The state parameter is a fundamental characterizing parameter for soils (Been & Jefferies, 1985) that represents the difference between the current (e) and void ratio (e_c) at the critical state. The NorSand model includes associated plasticity and allows dilation, similar to that observed in natural soil, by introducing limited hardening. This limited hardening causes yielding in unloading conditions, replicating observed soil behaviour with second-order detail.

2. Materials and methods

The activities involved in mining and processing iron ore on site are shown in the flow chart in Figure 1. Ore processing ranges from simple crushing and screening methods to more sophisticated processes to upgrade the ore quality. These are physical processes that remove impurities by

segregating particles that have an anomalous particle density or gravity. After the screening stage, the fine material, with gradation below the sinter feed (particles diameters from 0.15 to 6.3 mm), moves on to the desliming stage through a sequence of hydrocyclone batteries to remove the finer material. After this stage, the slimes are stored in the TSF. The remaining material moves on to the reverse cationic flotation process, which isolates the fine-grained ore (pellet feed), and the flotation tailings are also stored in the TSF.

The procedure for collecting and preparing the samples investigated in this study was conducted in two phases: (1) The tailings samples were collected at the exit of iron ore beneficiation plants (IBPs, Plant 1 and Plant 2). In this case, to reduce the influence of fluctuations in the plant's operation, the samples were composed of subsamples collected over three weeks every other day. (2) Preparation of tailings blends from Plant 1 in a mixer by adding 60% flotation tailings from Plant 2.

The tailings produced at the IBPs considered here were mainly composed of silica and iron, as shown in Table 1. FT-P1 and FT-P2 were disposed of in the same TSF without deposition of slimes. Figure 2 shows an optical microscopy image of the flotation iron ore tailings. The aim of this research was to investigate the mechanical behaviour of tailings at the TSF. Thus, composite samples BL-2&1 had the same composition proportions. In this paper, the BL-2&1 composite material was considered representative of the tailings in a TSF.

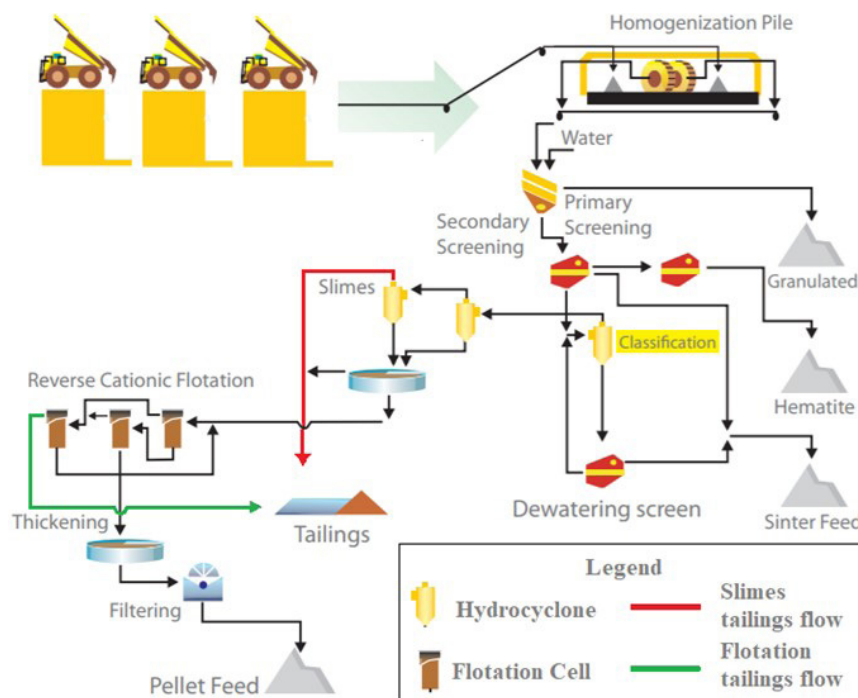


Figure 1. Simplified flow chart showing typical iron ore processing (Silva et al., 2021).

The preliminary stage of this study involved tailings characterization. The laboratory tests included tests to determine the general chemistry, calcination loss, specific gravity, grain size distribution, Atterberg limits, and standard Proctor parameters. Instead of using the conventional relative density test (maximum and minimum void ratio), the Brazilian mining industry has been applying the Proctor test as a standard to control the density of tailings at TSFs. There is empirical evidence showing that the void ratio (e) determined in the field can be out of the range corresponding to standard laboratory relative density testing (Lunne et al., 2019).

According to ASTM guidelines, these tailings are typically fine grains of industrial silt sands with minimal or

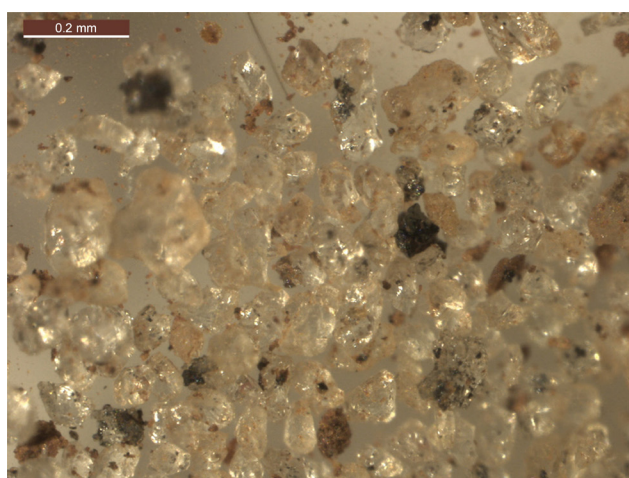


Figure 2. Optical microscopy of flotation iron ore tailings.

Table 1. Chemical composition of the tailings studied and calcination losses.

Chemical composition (%)	Tailings	
	FT-P1	FT-P2
Fe	25.44	13.48
SiO ₂	61.23	80.22
P	0.027	0.016
Al ₂ O ₃	0.79	0.028
Mn	0.021	0.001
TiO ₂	0.058	0.001
CaO	0.017	0.007
MgO	0.91	0.16
Calcination losses	0.91	0.16

no plasticity. The e_{max} and e_{min} of the flotation tailings are approximately 1.1 and 0.6, respectively. Table 2 summarizes the basic geotechnical properties of the flotation and composite tailings samples. The specific gravity ranges from 3.2 to 3.8, which is consistent with typical metal tailings but much higher than that of natural soils. This table also shows the typical characteristics of nine flotation tailings from QF (Silva et al., 2013); the data are from nine IBPs that predominantly process haematite ore. Notably, this work intends to evaluate the ability of NorSand to predict the behaviour of granular iron ore tailings. It is not the intention of this study to represent a specific deposit.

Figure 3 shows the grain-size distributions of BL-2&1, which are the flotation tailings used to create the blend and slime tailings from Plant 1 for comparison. Figure 3 also shows data on iron ore tailings from Silva et al. (2013). Currently, IBPs process itabirite, which has a lower Fe content and generates finer tailings than iron does. According to the Unified Soil Classification System, these tailings are silty or silty sand. NorSand is a mathematical framework that is validated across a wide range of soil types. All these iron ore tailings have grain sizes within NorSand's limits verified by Jefferies et al. (2015); as shown on Figure 3.

Triaxial tests were conducted to investigate the dilatancy and critical state behaviour of BL-2&1. A triaxial testing system was used to conduct consolidated undrained (CU) and consolidated drained (CD) triaxial compression tests on the tailings according to ASTM standards D4767-11 and D7181-11, respectively. The testing programme involves dense specimens (four CD tests) and loose specimens (four CD and four CU tests). The triaxial test specimens were 3.91 cm in diameter and 8 cm in height. The dense specimens were remoulded to reach approximately 105% of the maximum dry density identified via Proctor test. In contrast, the loose specimens were compacted to approximately 75% of the Proctor test density.

A relevant aspect of reconstitution is that it can achieve a uniform density throughout the specimen. Therefore, moist tamping and compaction techniques were adopted to obtain six equal volume layers. For the loose specimens, it was only necessary to place the tamper and apply a light load before the layer reached the specified thickness. On the other hand, for the dense specimens, it was necessary to also use a Harvard miniature compaction apparatus (Figure 4). This compaction tamper consists of a metallic cylinder with a spring inside, which is compressed during the compaction process.

Table 2. Basic geotechnical parameters of iron ore tailings from the Brazilian QF.

Tailings	G_s	Void ratio		Standard Proctor		Atterberg limits			Classification
		e_{min}	e_{max}	ρ_d (kN/m ³)	w (%)	LL	PL	PI	
FT-P1	3.8	0.59	1.13	19	14		NP		ML
FT-P2	3.2	0.6	1.1	18	14		NP		ML
BL-2&1	3.6	0.85	1.31	22	12		NP		ML
Typical	3-4.2			17-19	11-15		NP		ML

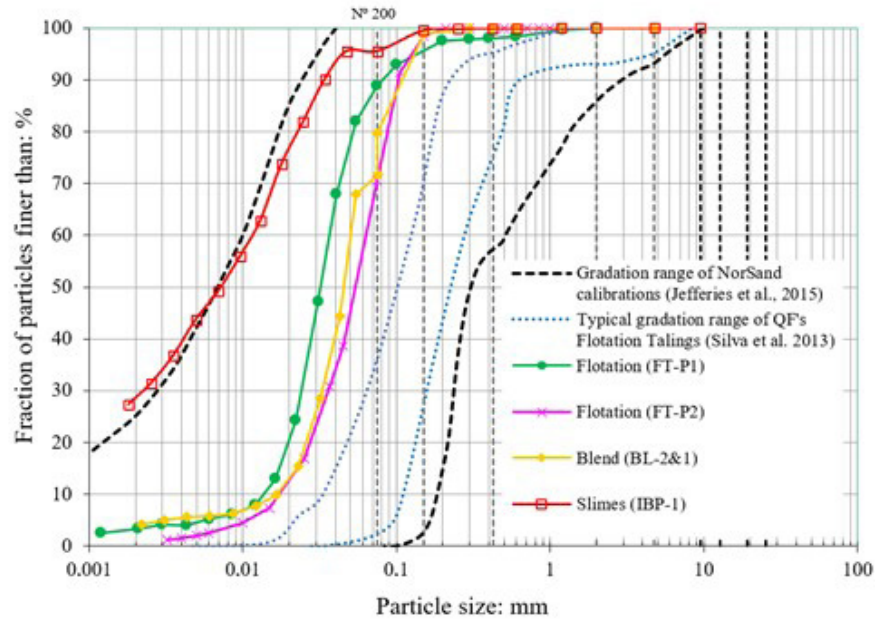


Figure 3. Grain size distributions of iron ore tailings from the Brazilian QF.



Figure 4. Dense specimen preparation method.

The saturation of the specimens was achieved by flushing de-aired water through the specimens. This process did not result in full saturation. Thus, the water pressure was increased gradually, and the degree of saturation was checked by the ‘B-test’ (Skempton’s B value > 95%). According to Verdugo & Ishihara’s (1996) proposal, an additional consolidation step was applied at the end of the test (after shear) to generate apparent cohesion and make it feasible to handle the specimens without material loss. This made it possible to determine void ratio (e) from the final moisture content and volume measured. This corresponds to ASTM method B, with the adjustments proposed by Verdugo & Ishihara. Freezing was not performed at the end of the test.

Bender element (BE) tests have gained popularity in recent years and are rapidly extending from research to practice. The BE values of the shear modulus (G) are usually chosen as a starting point for calibration. In practice, the value introduced by the NorSand calibration of CU triaxial tests has been proportional to but lower than the value measured by geophysical methods.

In such an analysis, it is helpful to divide the soil behaviour into distortional and volumetric strains. Moreover, for soils, it is convenient to represent elasticity in terms of the shear modulus (G) and bulk modulus (K). Equations 2 and 3 show the relation between these parameters:

$$G = E / [2(1+\nu)] \quad (2)$$

$$K = E / [3(1-2\nu)] \quad (3)$$

where E is Young's modulus and ν is Poisson's ratio. NorSand assumes a constant Poisson's ratio, so there is a direct link between K and G . Bellotti et al. (1996) performed extensive testing to investigate the elasticity of Ticino sand and measured Poisson's ratios between 0.1 and 0.3.

The shear modulus (G_{max}) and its variation with both e and confining stress were measured in a triaxial cell by performing isotropic consolidation tests with BEs. After determining the critical state and the dilatancy parameters of the BL-2&1 tailings, the model was calibrated using the free software NorTxl (Jefferies & Been, 2016). The aim of the calibration was to establish parameters that best represent the selected flotation tailings. Subsequently, more advanced numerical simulations were performed on the commercial numerical modelling platform FLAC3D. The NorSand model was implemented as a user-defined model on this platform. FLAC3D version 6.0 was customized to incorporate the NorSand model and was developed in a partnership between ITV (Instituto Tecnológico Vale) and Itasca. After that, Itasca incorporated this development into Version 7 of its software. The development documentation is attached to this paper, including the source code implemented in C++ and the DLL files.

3. Mechanical properties of the tailings

3.1 Triaxial tests

Table 3 shows the physical properties of the BL-2&1 tailings specimens. There was some difference between the moulding

conditions specified and obtained, so the values were slightly lower than those reported in section 2. Figures 5 and 6 show compressive triaxial test results under both dense and loose conditions. These figures also show the axial strain against the deviatoric stress and the mean effective stress. Figure 5 shows the derived critical state line (CSL) obtained from the post-peak portion of the undrained tests of the loose specimens. Some specimens appear to reach a steady state at approximately 6% strain but then dilate at higher strains. The quasi-steady state in this test must not be understood as a critical state but instead as a transient condition under which the specimens transition from contractive to dilative behaviour.

3.2 Critical state and dilatancy (model calibration)

Figure 6 shows the state diagram of eight drained and four undrained triaxial compression tests. These data have been used to estimate the CSL shown in Figure 7. One critical state theory axiom is that the soil state moves to the critical state with increasing shear strain. In the Figure 7, it is possible to observe this phenomenon in the results for both dense and loose samples. However, in the four dense CD tests, the deformation required to reach the CSL is outside the practicable limits of the triaxial assembly. A conventional semilog idealisation of the CSL can be fitted to the data using the properties $\Gamma = 1.28$ and $\lambda_{10} = 0.19$. Occasionally, this semilog trend is not a particularly good representation of the CSL, and an improved CSL is given by power-law idealisation with $C_a = 1.13$, $C_b = 0.23$, and $C_c = 0.27$. Over the stress range of the data (approximately 60-2000 kPa), both models are equally suitable within a precision of approximately $e = \pm 0.02$. The semi-log CSL has the advantage of the least number of parameters; on the other hand, many workers applying critical state models prefer the power-law CSL, so this is the reason for presenting both.

Table 3. Triaxial tests on the BL-2&1 tailings: physical properties of the specimens.

Specimen			Initial			Post-consolidation	
Test	Condition	Test type	γ (kN/m ³)	γ_d (kN/m ³)	w (%)	Mean effective stress (kPa)	Void ratio (e)
1	dense	CD	24.5	22.6	8.74	50	0.67
2	dense	CD	24.4	22.5	8.68	100	0.64
3	dense	CD	24.6	22.6	8.82	150	0.62
4	dense	CD	24.5	22.6	8.65	300	0.55
5	loose	CD	17.6	16.7	5.38	100	0.92
6	loose	CD	17.6	16.7	5.56	300	0.85
7	loose	CD	17.7	16.7	5.61	400	0.8
8	loose	CD	17.6	16.6	5.34	600	0.78
9	loose	CU	17.7	16.7	5.9	100	0.94
10	loose	CU	17.6	16.7	5.44	200	0.87
11	loose	CU	17.6	16.7	5.44	400	0.86
12	loose	CU	17.7	16.7	5.61	600	0.84

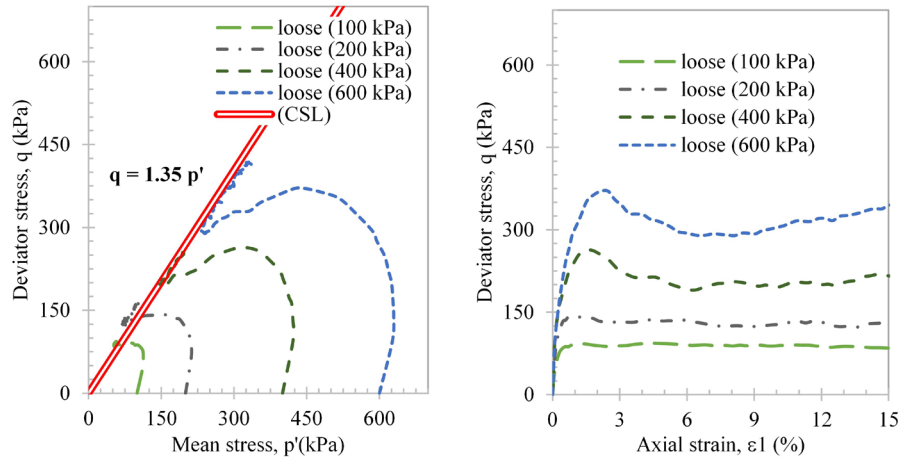


Figure 5. CU triaxial test – loose specimens.

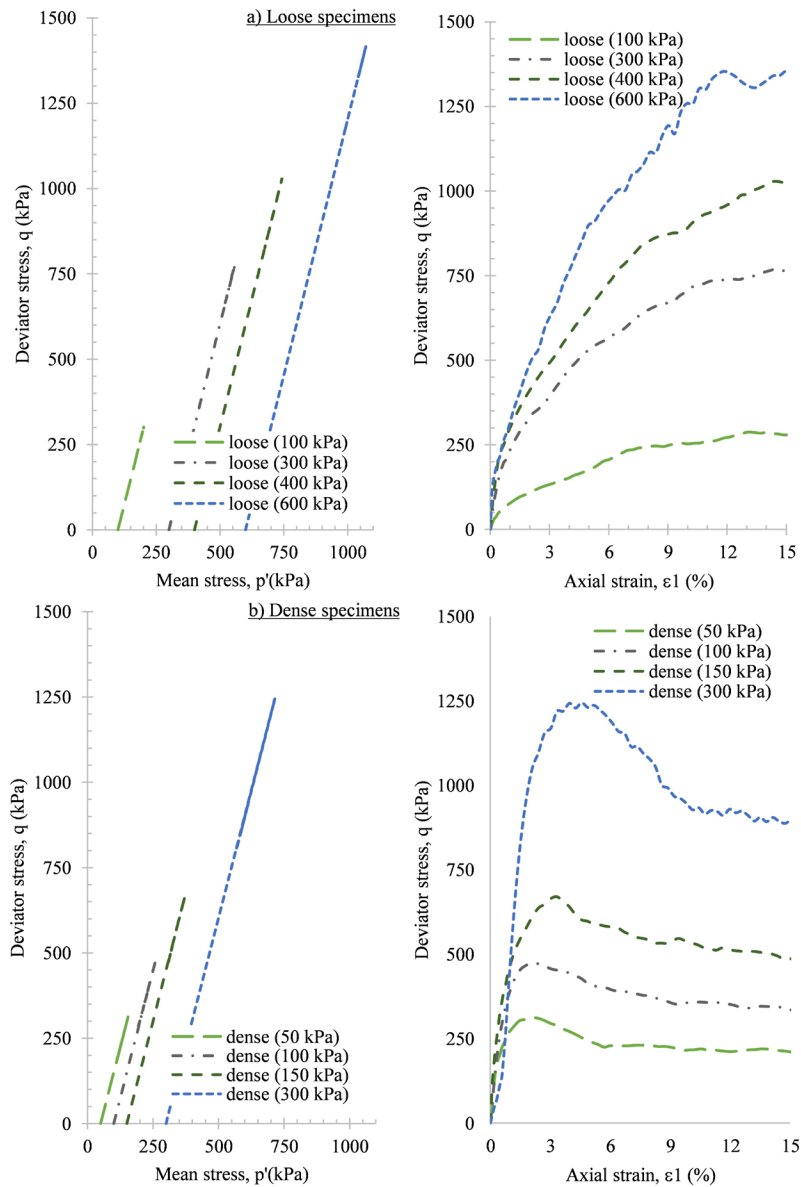


Figure 6. CD triaxial test stress path: (a) loose specimens; (b) dense specimens.

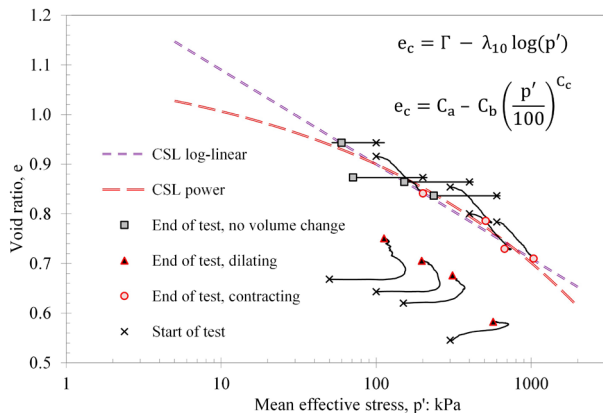


Figure 7. State diagram of triaxial test results with the corresponding log-linear and power-law CSL.

Figure 8 shows the maximum stress ratio η_{max} measured against the peak dilation of BL-2&1. Equation 4 shows the flow rule from Nova & Wood (1982), which was fitted to determine the critical stress ratio ($M_{tc} = 1.35$) and the parameter N_{tc} (0.20) of work dissipation by plastic volumetric strain (Nova & Wood, 1982; Jefferies & Been, 2016).

$$\eta_{max} = M_{tc} - (1 - N_{tc}) D_{min} \tag{4}$$

The stress ratio (η) and the equivalent dilatancy (D) were obtained by triaxial compression. The M_{tc} value determined in the CD tests is similar to that inferred from Figure 8.

Equation 5 is the state–dilatancy law proposed by Been & Jefferies (1985):

$$D_{min} = \chi_{tc} \psi \tag{5}$$

The state–dilatancy parameter χ_{tc} is obtained by plotting the maximum dilation versus ψ at maximum dilation. The determination of this law for BL-2&1 is shown in Figure 9. The trend line with $\chi_{tc} = 3.9$ is forced to intercept zero (a theoretical requirement):

3.3 Elasticity and plasticity

The five parameters (Γ , λ , M , N , and χ) defined thus far reflect the intrinsic behaviour of soil and its relationship between the current state and the critical state. Typically, parameters are defined from triaxial compression tests, and the subscript TC is used. These are not parameters of the NorSand model but a set of fundamental characteristics shared by many critical state soil mechanics models. Other parameters will be necessary for adequate representation of the deformational behaviour of any soil. Henceforth, the elastic and plastic properties were identified with numerical calibration.

The calibration of the plasticity and elastic parameters was performed according to the methodology proposed by

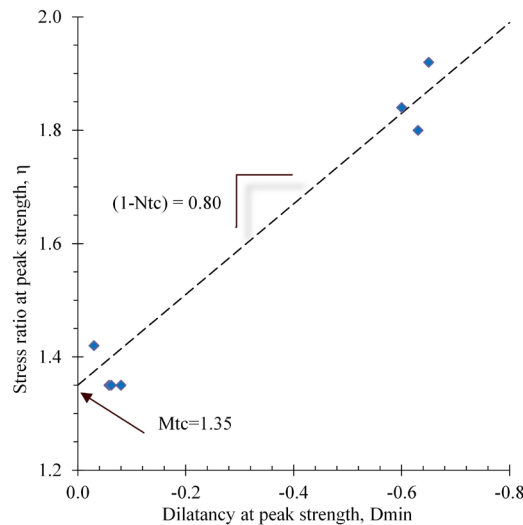


Figure 8. Stress–dilatancy of BL-2&1 at peak strength (η_{max} versus D_{min}).

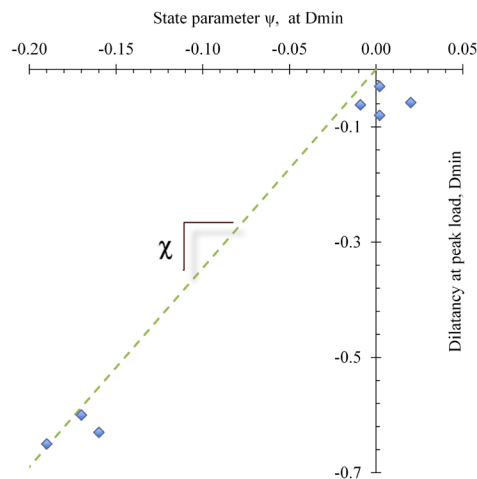


Figure 9. State–dilatancy of BL-2&1 at peak load (D_{min}). Note: theory requires trend to pass through the origin.

Jefferies & Been (2016). The dimensionless modulus H is a plastic hardening parameter in NorSand. The software NorTx1 (Excel VBA) allows for determining the parameter H by optimizing a set of drained triaxial test data. In this process of iterative forward modelling (IFM), an initial value of H is guessed, and the theoretical stress–strain behaviour is computed using NorSand (Jefferies & Been, 2016). Other soil properties are kept fixed. A trend is generally found in the form of

$$H = H_0 - H_y \psi \tag{6}$$

Some variability arises among tests because fabric effects are not included in the constitutive model. The H relation in Equation 6 provides a good fit across the suite

of BL-2&1 tests with the properties $H_0 = 85$ and $H_y = 850$, as shown in Figure 10.

Elasticity is essential to consider understanding how the undrained strength and stiffness of this material develop. Although elastic behaviour used to be challenging to measure, the advent of geophysical methods has made elastic measurements routine in practice in the laboratory and in situ.

The elastic shear modulus was determined with BE testing, and the results fit a power law. For dense samples, the proportionality constant and the exponent are 70 and 0.53, respectively; For loose samples, the best fit was obtained with

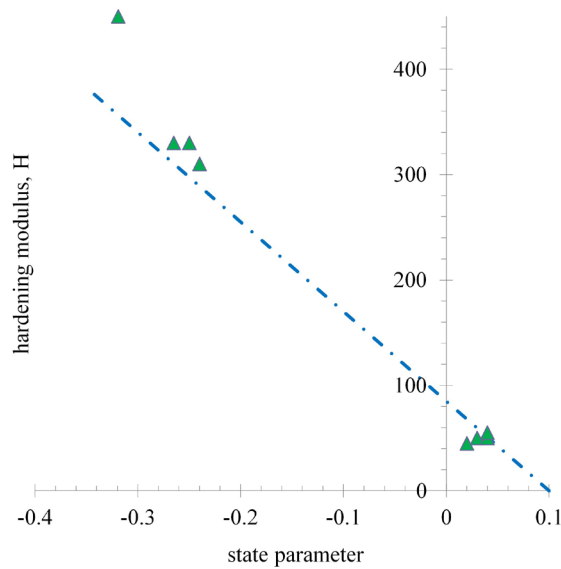


Figure 10. Fit across the BL-2&1 tailings (properties $H_0 = 85$ and $H_y = 850$).

39 and 0.6. The fit of the elastic model to the measured data using these soil properties is shown in Figure 11. Poisson's ratio was not measured, and a value of 0.2 was assumed for modelling.

3.4 NorSand performance validation

The properties of BL-2&1 derived from the drained and undrained triaxial tests are summarized in Table 4. The drained triaxial tests for loose and dense BL-2&1 tailings are presented in Figures 12a and 12b, respectively. In Figure 12a, it is possible to see that both the stress/strain graphs and the volumetric strain/axial strain graphs indicate the models'

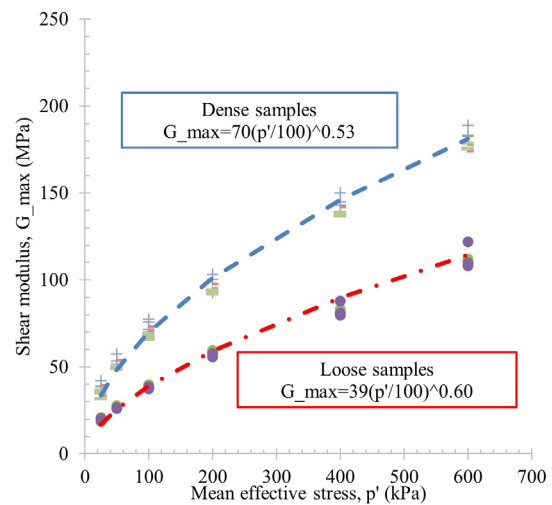


Figure 11. Variation of G_{max} with p' .

Table 4. NorSand soil properties of the BL-2&1 tailings and the typical range for sands.

	BL-2&1	Typical range (*)	Comment
CSL			
Γ	1.28	0.9–1.4	'Altitude' of CSL defined at 1 kPa
λ_{10}	0.19	0.03–0.15	Slope of CSL defined on base 10
CSL_a	1.13	-	Parameter for curved CSL analogous to Γ
CSL_b	0.23	-	Parameter for curved CSL analogous to λ
CSL_c	0.27	-	Parameter for curved CSL analogous to an exponent of the stress level
Plasticity			
M_{tc}	1.35	1.2-1.5	Critical friction ratio, with triaxial compression as a reference condition
N_{tc}	0.20	0.2-0.5	Volumetric coupling parameter
χ_{tc}	3.45	2.5-4.5	Relates minimum dilatancy to corresponding ψ , with triaxial as a reference condition
H	n/a	50-500	Plastic hardening modulus for loading
H_0	85	-	Often equal to $f(\psi)$
H_ψ	850	-	$H = H_0 - H_\psi \cdot \psi$
Elasticity			
G	39 and 70	-	Shear modulus
G_{exp}	0.6 and 0.53	-	Soil property
ν	0.2 (adopted)	0.1-0.3	Poisson's ratio

(*) NorSand typical range for sands (Jefferies et al., 2015).

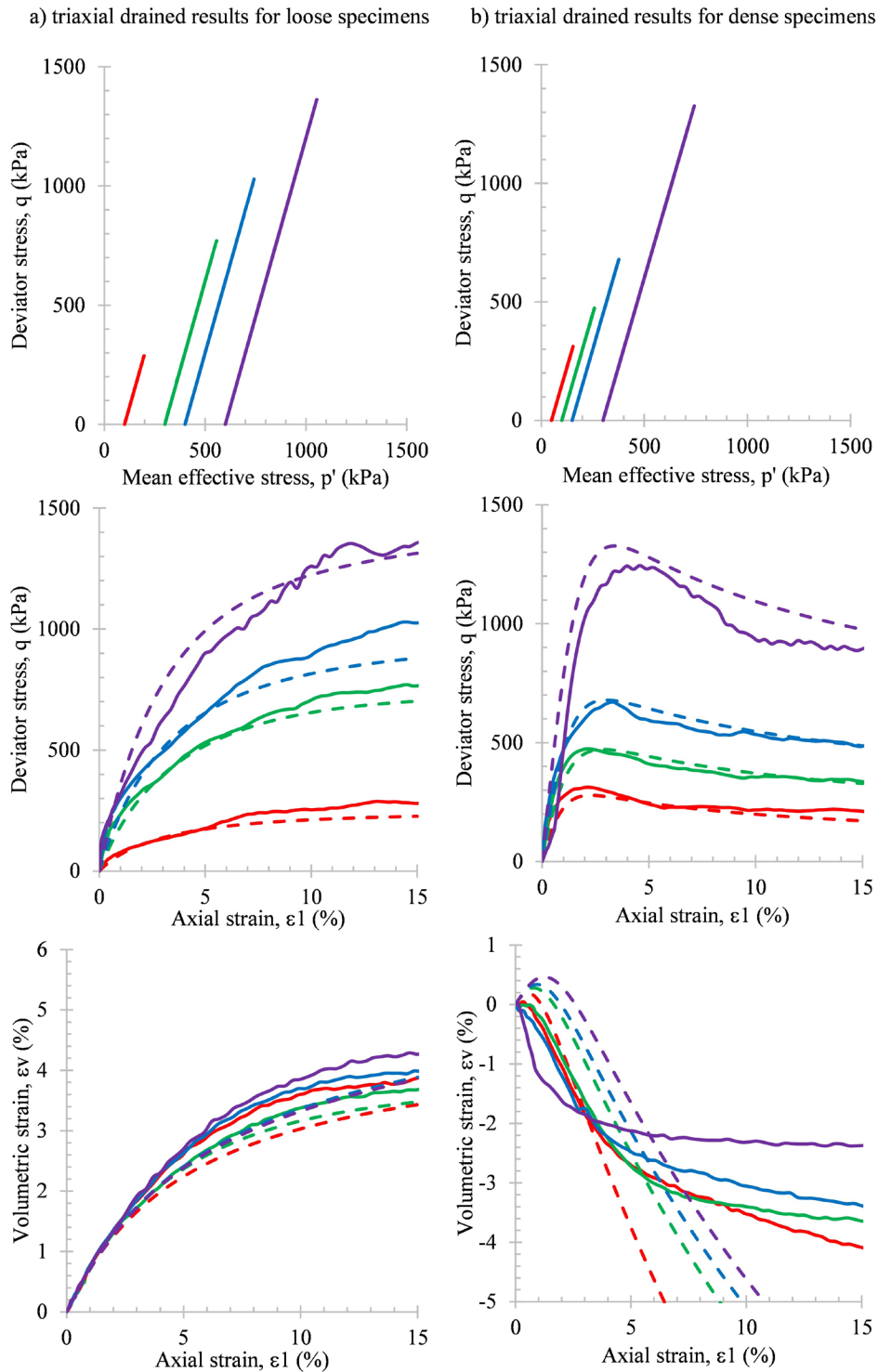


Figure 12. Drained triaxial test on samples and flotation tailings: calibrations of NorSand for the BL-2&1 sample: (a) loose specimens; (b) dense specimens. Continuous and dashed lines represent experimental and numerical results, respectively.

adherence to the experimental data. On the other hand, for dense specimens (Figure 12b), there is good adherence between only the experimental and numerical stress/strain curves. However, the relationship between axial and volumetric deformations shows adherence only until the peak deviator

stress. After reaching this value, the experimental volumetric deformation is reduced considerably and diverges from the model results. This divergence may be associated with the formation of shear bands and limitations of the boundary conditions defined in the modelling (Oda & Kazama, 1998).

Figure 13 shows two tailings specimens after drained shear. The well-defined rupture plane in Figure 13b is experimental evidence of the shear band hypothesis. The Txl2 software (VBA code) implements the NorSand model as a single Cauchy stress tensor, so shear bands are not allowed in this implementation. To assess the hypothesis of localization, complementary analyses were performed with the NorSand UDM for FLAC3D software.

Figure 14 shows the simulated triaxial tests for loose and dense conditions (i.e., ψ of 0.2 and -0.27, respectively). Cylindrical specimens were modelled with a 3.7 cm diameter and 8-cm height and sheared up to 20% deformation at a constant speed. The effective confining stress was fixed at 100 kPa. The horizontal displacement at the top and bottom was restricted to simulate the nonlubricated test conditions.

Despite the inaccuracy of the boundary conditions, the simplicity of the mesh, and the lack of proper calibration,

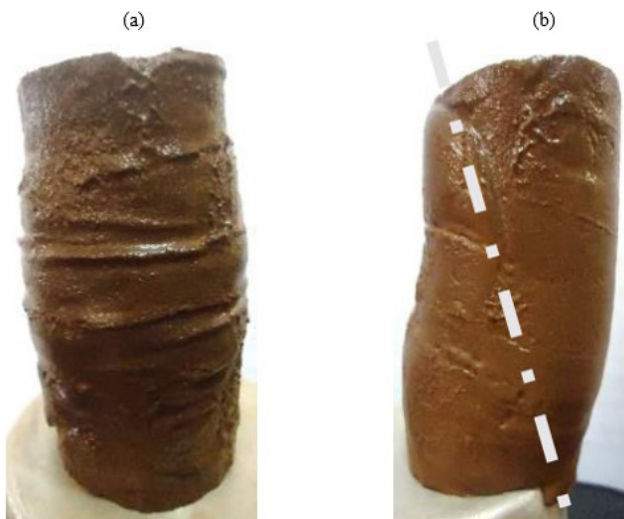


Figure 13. Photographs of two specimens (a) loose and (b) dense sheared in a drained triaxial test.

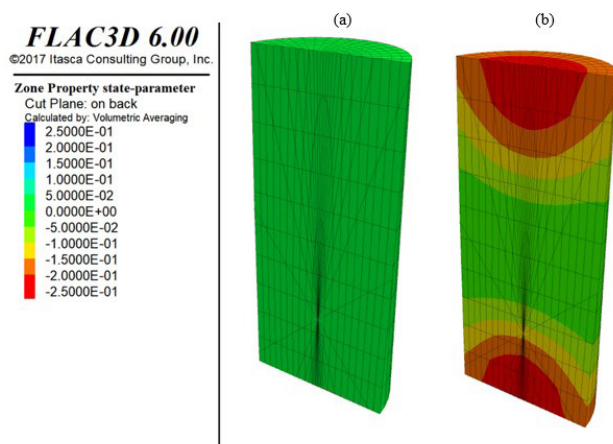


Figure 14. 3D numerical simulation of drained triaxial tests with compaction of approximately (a) 78% and (b) 105% of the standard Proctor dry density.

insightful observations can be made. First, the loose specimen was in a critical state condition in the shearing phase, and second, the dense specimen also converged to a steady state, but only the middle portion reached the critical state condition. Third, there is a notable anisotropy of the specimen results in this last case. These findings are consistent with the experimental observations and support the hypothesis that shear bands tend to form in dense samples.

Finally, Figure 15 shows the experimental results against the numerical predictions of the undrained tests for the loose samples. Again, the adherence of the numerical results to the experimental data is acceptable. However, the experimental results of the two specimens indicated that the strength increased at larger deformations (with a threshold of approximately 10% axial deformation). The increase in apparent strength during the tests is not predicted by the NorSand model. This may be associated with a boundary condition at large deformation in the tests. In other words, the specimens' loss of symmetry in the test influences the results. Figure 16 shows a post-rupture photograph of a specimen consolidated at 600 kPa. An increase in the specimen's central section is evident, corroborating the hypothesis of loss of symmetry at a large deformation.

4. Conclusion

This study critically evaluated the predictive capacity of NorSand, a critical state model, to represent the behaviour of iron ore tailings from the QF in Minas Gerais. Additional characterization of the tailings soils was presented to provide a broader description of the materials. The selected model

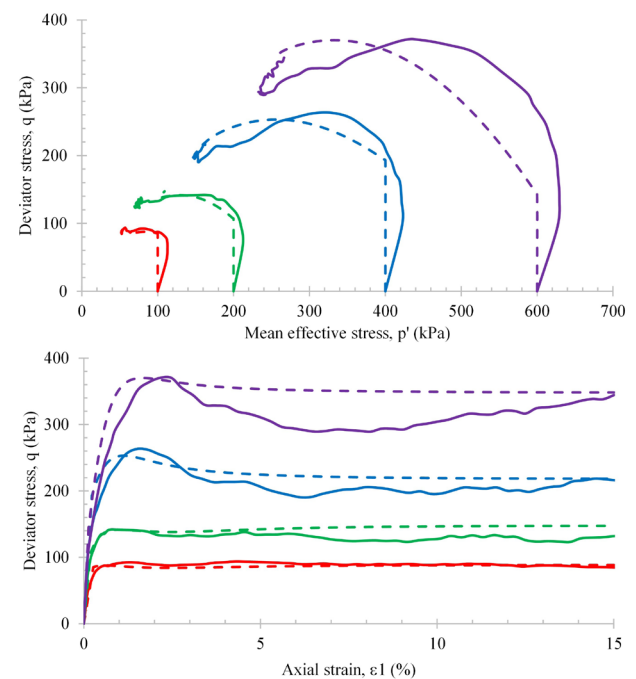


Figure 15. Comparison between experimental (continuous lines) and numerical (dashed lines) results: undrained triaxial test of a loose sample of BL-2&1 tailings.



Figure 16. Photograph of the undrained triaxial test result of a loose specimen (~78%) of flotation tailings (BL-2&1).

was adequate to evaluate the behaviour of these mine tailings. There was a consistent adherence of the simulation results to the experimental results of drained and undrained tests for deformations below 5% and specimens in which the state parameter had a small magnitude.

The predictions of the volumetric deformation model did not adhere to the experimental observations for dense drained tests, particularly after reaching the peak strength. This divergence may be associated with the appearing of shear bands. A multielement simulation showed that the formation of shear bands occurs in only dense specimens, which is coherent with the suggested hypothesis. Additional studies are needed to elucidate this issue.

Acknowledgements

The authors would like to acknowledge the University of Brasilia (UnB) and the professors of the Graduate Program in Geotechnics at UnB for the knowledge provided. The present research was intended to test the validity of the NorSand model and verify its applicability to granular iron ore tailings. To achieve this goal, NorSand was implemented as a new user-defined constitutive model (UDM) in FLAC3D (Itasca, 2016). The model implemented was NorSand in its static (NorSand-M, monotonic) and dynamic (NorSand-PSR, with principal stress rotation) forms. As a sponsor of our research, Vale Institute of Technology (ITV) hired Itasca, the platform's developer, to implement a new numerical model as a UDM in FLAC3D. To contribute effectively and broadly to the practice of engineering, ITV abdicated the development rights and intellectual property. The authors would like to thank ITV for this effort.

Declaration of interest

The authors have no conflicts of interest to declare. All co-authors have observed and affirmed the contents of the paper, and there is no financial interest to report.

Authors' contributions

João Paulo de Sousa Silva: conceptualization, data curation, methodology, visualization, writing – original draft. Pedro Pazzoto Cacciari: formal analysis, validation. Vidal Felix Navarro Torres: validation. Luís Fernando Martins Ribeiro: supervision, formal analysis, methodology. André Pacheco de Assis: supervision, validation, writing – review & editing.

List of symbols

BL-2&1	blended tailings from iron ore operation plants 2 and 1
C_a	parameter for curved CSL analogous to Γ
C_b	parameter for curved CSL analogous to λ
C_c	parameter for curved CSL analogous to an exponent of the stress level
CD	consolidated drained triaxial compression tests
CSL	critical state line or critical state locus
CU	consolidated undrained triaxial compression tests
D	dilatancy
DLL	Dynamic-link library is Microsoft's implementation of the shared library concept in the Microsoft Windows and OS/2 operating systems.
E	Young's modulus
FT	flotation tailings from iron ore operation
FT-P1	flotation tailings from iron ore operation plant 1
FT-P2	flotation tailings from iron ore operation plant 2
G	shear modulus
G_0	initial shear modulus
G_{max}	shear modulus (the 'max' subscript is currently used geotechnical practice to denote elasticity)
G_s	specific gravity
H	dimensionless modulus is a plastic hardening parameter in NorSand.
H_0	plastic hardening parameter
H_y	plastic hardening parameter
IBPs	iron ore beneficiation plants
IFM	iterative forward modelling
K	bulk modulus
LL	liquid limit
M	critical friction ratio
M_{tc}	critical friction ratio (with triaxial as a reference condition)
ML	low-plasticity silt
NorTxl	free software in VBA
NP	non-plastic
N_{tc}	volumetric coupling parameter
P1	mineral processing plant 1

P2	mineral processing plant 2
PI	plasticity index
PL	plastic limit
TSFs	tailings storage facilities
UDM	User Defined constitutive Models for Itasca software
USCS	Unified Soil Classification System
VBA	Visual Basic for Applications
e	void ratio of the soil
e_{max}	minimum void ratio of the soil
e_{min}	minimum void ratio of the soil
e_c	void ratio at the critical state
p'	mean effective stress
w	water content
Γ^*	Altitude' of CSL defined at 1 kPa
γ	dry density
γ_d	dry density
η	stress ratio, volumetric coupling parameter
η_{max}	stress ratio, volumetric coupling parameter
λ	slope of CSL
λ_{10}	slope of CSL defined on base 10
ν	Poisson's ratio
χ	state-dilatancy parameter
χ_{ic}	state-dilatancy parameter (relates minimum dilatancy to corresponding ψ , with triaxial as a reference condition)
ψ	state parameter

References

- Been, K., & Jefferies, M. (1985). State parameter for sands: Geotechnique V35, N2, June 1985, P99–112. *International Journal of Rock Mechanics and Mining Sciences & Geomechanics Abstracts*, 22(6), 198. [http://dx.doi.org/10.1016/0148-9062\(85\)90263-3](http://dx.doi.org/10.1016/0148-9062(85)90263-3).
- Bellotti, R., Jamiolkowski, M., Lo Presti, D.C.F., & O'Neill, D.A. (1996). Anisotropy of small strain stiffness in Ticino sand. *Geotechnique*, 46(1), 115-131. <http://dx.doi.org/10.1680/geot.1996.46.1.115>.
- Boulanger, R.W., & Ziotopoulou, K. (2015). *PM4Sand (version 3): A sand plasticity model for earthquake engineering applications, Report No. UCD/CGM-15/01*. Center for Geotechnical Modeling, Department of Civil and Environmental Engineering, University of California.
- Casagrande, A. (1976). *Liquefaction and cyclic deformation of sands-a critical review: Harvard Soil Mechanics Series No. 88*. Harvard University.
- Dafalias, Y. (1986). Bounding surface plasticity. I: mathematical foundation and hypoplasticity. *Journal of Engineering Mechanics*, 112(9), 966-987. [http://dx.doi.org/10.1061/\(ASCE\)0733-9399\(1986\)112:9\(966\)](http://dx.doi.org/10.1061/(ASCE)0733-9399(1986)112:9(966)).
- Dafalias, Y., & Manzari, M. (1997). A critical state two-surface plasticity model for sands. *Geotechnique*, 47(2), 255-272. <http://dx.doi.org/10.1680/geot.1997.47.2.255>.
- Dafalias, Y., & Manzari, M. (2004). Simple plasticity sand model accounting for fabric change effects. *Journal of Engineering Mechanics*, 130(6), 622-634. [http://dx.doi.org/10.1061/\(ASCE\)0733-9399\(2004\)130:6\(622\)](http://dx.doi.org/10.1061/(ASCE)0733-9399(2004)130:6(622)).
- Dafalias, Y., & Popov, E. (1975). A model of nonlinearly hardening materials for complex loading. *Acta Mechanica*, 21, 173-192. <http://dx.doi.org/10.1007/BF01181053>.
- Davies, M. (2002). Tailings impoundment failures: are geotechnical engineers listening? *Geotechnical News – Vancouver*, 20(3), 31-36.
- Dorr, J.V.N. (1969). *Physiographic, stratigraphic and structural development of the Quadrilátero Ferrífero, Minas Gerais, Brazil (No. 641-A, pp. A1-A110)*. US Government Printing Office. <https://doi.org/10.3133/pp641A>.
- Jefferies, M. (1993). Nor-Sand: a simple critical state model for sand. *Geotechnique*, 43(1), 91-103. <http://dx.doi.org/10.1680/geot.1993.43.1.91>.
- Jefferies, M., & Been, K. (2016). Soil liquefaction: a critical state approach, 2nd edition. *Environmental Earth Sciences*, 75(12), 1014. <https://doi.org/10.1007/s12665-016-5600-y>.
- Jefferies, M., Shuttle, D., & Been, K. (2015). Principal stress rotation as cause of cyclic mobility. *Geotechnical Research*, 2(2), 66-96. <http://dx.doi.org/10.1680/gr.15.00002>.
- Li, W., Coop, M.R., Senetakis, K., & Schnaid, F. (2018). The mechanics of a silt-sized gold tailing. *Engineering Geology*, 241, 97-108. <http://dx.doi.org/10.1016/j.enggeo.2018.05.014>.
- Lunne, T., Knudsen, S., Blaker, Ø., Vestgård, T., Powell, J., Wallace, C.F., Krogh, L., Thomsen, N.V., Yetginer, G., & Ghanekar, R.K. (2019). Methods used to determine maximum and minimum dry unit weights of sand: is there a need for a new standard? *Canadian Geotechnical Journal*, 56(4), 536-553. <http://dx.doi.org/10.1139/cgj-2017-0738>.
- Nova, R., & Wood, D.M. (1982). A constitutive model for soil under monotonic and cyclic loading. In G.N. Pande & C. Zienkiewicz (Eds.), *Soil mechanics-transient and cyclic loads* (pp. 343–373). Wiley.
- Oda, M., & Kazama, H. (1998). Microstructure of shear bands and its relation to the mechanisms of dilatancy and failure of dense granular soils. *Geotechnique*, 48(4), 465-481. <http://dx.doi.org/10.1680/geot.1998.48.4.465>.
- Olivier, G., De Wit, T., Brenguier, F., Bezuidenhout, L., & Kunjwa, T. (2018). Ambient noise Love wave tomography at a gold mine tailings storage facility. *Geotechnique Letters*, 8(3), 178-182. <http://dx.doi.org/10.1680/jgele.18.00016>.
- Schnaid, F., Bedin, J., Fonseca, A.J.P.V., & Costa Filho, L.M. (2013). Stiffness and strength governing the static liquefaction of tailings. *Journal of Geotechnical and Geoenvironmental Engineering*, 139(12), 2136-2144. [http://dx.doi.org/10.1061/\(ASCE\)GT.1943-5606.0000924](http://dx.doi.org/10.1061/(ASCE)GT.1943-5606.0000924).
- Silva, J.P.S., Cacciari, P.P., Ribeiro, L.F., & Jefferies, M. (2021). Influence of compaction on small-strain shear modulus of iron ore tailings. In X. Geng (Eds.), *Proceedings of the Institution of Civil Engineers-Geotechnical Engineering* (pp. 1-30). London: Institution of Civil Engineers.
- Silva, J., Mendes, M., Milonas, J., Pirete, W., & Souza, W. (2013). Geotechnical parameters of iron ore tailings from the Quadrilátero Ferrífero after different treatments and

- ore processing. In R. Jewell, A.B. Fourie, J. Caldwell & J. Pimenta (Eds.), *Proceedings of the 16th International Seminar on Paste and Thickened Tailings* (pp. 261–271), Belo Horizonte, June 2013. Austrália: ACG. https://doi.org/10.36487/ACG_rep/1363_20_Silva.
- Soga, K., & Mitchell, J. (2005). *Fundamentals of soil behavior* (3rd ed.). Wiley.
- Verdugo, R., & Ishihara, K. (1996). The steady state of sandy soils. *Soil and Foundation*, 36(2), 81-91. http://dx.doi.org/10.3208/sandf.36.2_81.